



Facile one-step synthesis of N-doped carbon nanotubes/ N-doped carbon nanofibers hierarchical composites by chemical vapor deposition

Hua-Fei Li · Chen Wang · Long-Fei Liu · Ning Xie ·
Ming Pan · Ping Wu · Xiao-Di Wang · Zheling Zeng ·
Shuguang Deng · Gui-Ping Dai

Received: 19 July 2019 / Accepted: 5 December 2019 / Published online: 2 January 2020
© Springer Nature B.V. 2020

Abstract The composites consisting of nitrogen-doped carbon nanotubes (N-CNTs) and nitrogen-doped carbon nanofibers (N-CNFs) were fabricated using a mixture of nickel foam (template) and imidazole (solid precursor) in a facile one-step chemical vapor deposition (CVD) process. The morphology and microstructure of the N-doped carbon nanotubes/N-doped carbon nanofibers hierarchical composites (N-CNTs/N-CNFs) were determined by scanning electron microscopy, transmission electron microscopy, X-ray diffraction, Raman spectra, and X-ray photoelectron spectroscopy. The results indicated that the sample manifests regular hierarchical composites, great graphitization, and nitrogen doping. Furthermore, a probable growth mechanism is presented to analyze the composites.

Keywords N-doped carbon nanotubes · N-doped carbon nanofibers · One-step chemical vapor deposition · Solid precursor · Imidazole · Hierarchical nanocomposites

Introduction

3D hierarchical carbon nanomaterials, for example, CNTs/graphene, CNFs/graphene, and CNTs/CNFs, have received tremendous attention due to their extraordinary mechanical strength, thermal, and electrical properties (Su et al. 2017; Yan et al. 2013; Fan et al. 2010; Dong et al. 2013; Zhao et al. 2013; Kim et al. 2014; Peter et al. 2016; Zhang et al. 2018). As the typical 2D carbon nanomaterials, carbon nanotubes (CNTs) and carbon nanofibers (CNFs) have distinct merits, such as excellent mechanical strength, outstanding surface-to-volume ratio and high electrical conductivity. Therefore, they are promising choices in many applications such as batteries, supercapacitors, and energy storage (Landi et al. 2009; Zeng et al. 2014; Zhang et al. 2016). However, due to the existence of interfacial p-p interaction or the van der Waals' forces, those carbon nanostructures are easily agglomerated and stacked during the synthesis process and their electrochemical performances are inevitably lower than the theoretical predictions (Kim et al. 2012). In order to further overcome these shortcomings, various synthetic strategies and approaches have been attempted to acquire 3D carbon nanotubes/carbon nanofibers hierarchical composites. These special hierarchical composites not only effectively alleviate the agglomeration and stacking of CNTs and CNFs but also provide a large number of transport channels for electrons and ions between the CNTs and CNFs (Wang et al. 2015). Consequently, the 3D carbon nanotubes/carbon nanofibers hierarchical composites accordingly exhibit synergistic effects relative to the simple 2D structure of CNTs or CNFs

H.-F. Li · L.-F. Liu · N. Xie
School of Materials Science and Engineering, Nanchang
University, Nanchang 330031 Jiangxi, China

C. Wang · M. Pan · P. Wu · X.-D. Wang · Z. Zeng ·
G.-P. Dai
Department of Chemical Engineering, School of Environmental
and Chemical Engineering, Nanchang University,
Nanchang 330031 Jiangxi, China
e-mail: nanodai@gmail.com

S. Deng
School for Engineering of Matter, Transport and Energy, Arizona
State University, Tempe, AZ 85287, USA
e-mail: Shuguang.Deng@asu.edu

and show promising applications in the fuel cell (Hou and Reneker 2004), batteries (Park et al. 2013), and supercapacitors (Guo et al. 2009).

So far, several studies have reported the fabrication of 3D carbon nanotubes/carbon nanofibers hierarchical composites. Among those approaches, chemical vapor deposition appears to be a widespread and effective way to fabricate the hierarchical composites composed of CNTs and CNFs. Nevertheless, the reported 3D carbon nanotubes/carbon nanofibers hierarchical composites are typically prepared by a multistep CVD route, which first needs electrospinning technique and post-carbonization for the preparation of CNFs, and subsequently, the use of toxic organic gases as the carbon source for the growth of CNTs. For example, Wang et al. (2015) have reported a CVD method using C_2H_4 as the carbon source for the synthesis of carbon nanotube/carbon nanofiber hierarchical composites. Hou and Reneker (2004) have fabricated the CNT/CNFs via a CVD process using electrospun Fe nanoparticles-loaded carbon nanofibers as a substrate and hexane as the carbon source of CNTs. Especially, the stable and suitable catalysts that always need complex pretreatment is vital to the construction of 3D carbon hybrids in the previous reports (Park et al. 2013; Guo et al. 2009, 2014). Therefore, it is more desirable that CNFs/CNTs hybrid could be prepared by a simple one-step CVD technique. Simultaneously, nitrogen, an attractive heteroaromatic dopant, is always used to further tailor the chemical properties of sp^2 carbon materials (Sheng et al. 2011; Yang et al. 2015; Zhang et al. 2013). As a “neighbor” of carbon, nitrogen is chemically relatively easy to incorporate into the lattice of carbon materials due to the similar atomic radius compared with other heteroatoms (Paraknowitsch and Thomas 2013). Moreover, nitrogen doping can form disordered carbon structure and generate extrinsic defects, leading to an enhanced electronic conductivity (Ding et al. 2016; Song et al. 2016; Liu et al. 2013) and various approaches have been reported to obtain the nitrogen-doped carbonaceous materials. For example, Ghosh et al. (2010) achieved the goal of preparing highly nitrogen-doped CNTs by using imidazole as precursor. Guo et al. have used toluene or pyridine as the nitrogen and carbon source of the nitrogen-doped CNTs/CNFs composite (Guo et al. 2014). However, the N-CNTs/N-CNFs synthesized by using imidazole as a single carbon and nitrogen source has not been reported before. Hence, it would be quite

superior to synthesize such a 3D hierarchical composite in a one-step CVD method involving the simultaneous growth of N-CNTs and N-CNFs by using imidazole on a single metal substrate.

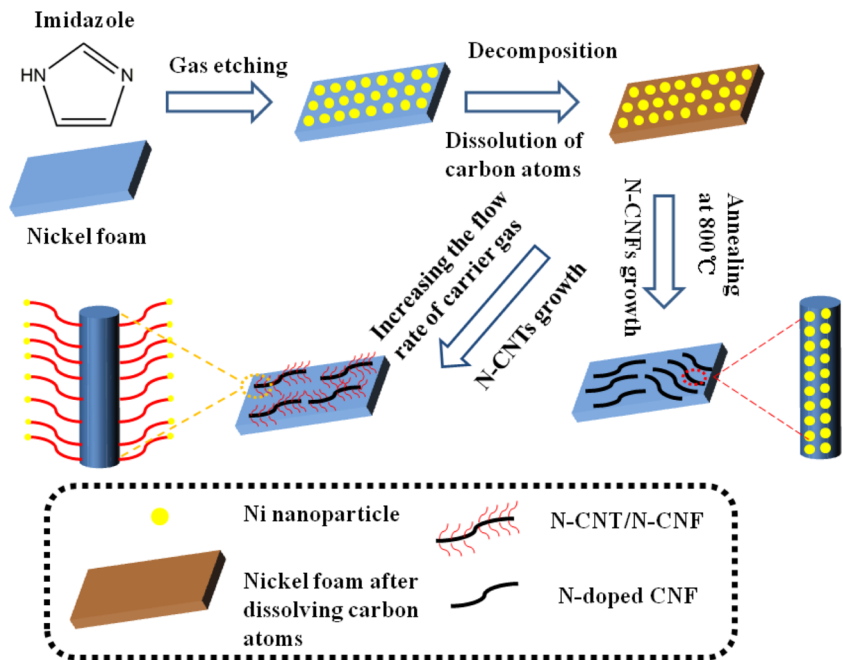
Herein, we report for the first time a successful direct synthesis of N-CNTs/N-CNFs in a one-step CVD method, where both N-doped carbon nanotubes and N-doped carbon nanofibers grow simultaneously on the nickel foam without adding any other metal or no-metal catalysts. In the work, we use imidazole, a nitrogen-containing aromatic rings carbon precursors, as a dual supplier of carbon and nitrogen of nitrogen-doped carbonaceous structure. The nickel foam (NF) not only serves as the substrate for the growth of N-CNTs and N-CNFs, but also offers in situ generated Ni nanoparticles (Ni NPs) as a catalyst during the synthesis process. Moreover, Ar was introduced as a carrier gas in the synthesis process and it is worth noting that changes in gas flow rate have a great influence on the morphology of N-CNTs/N-CNFs.

Experimental details

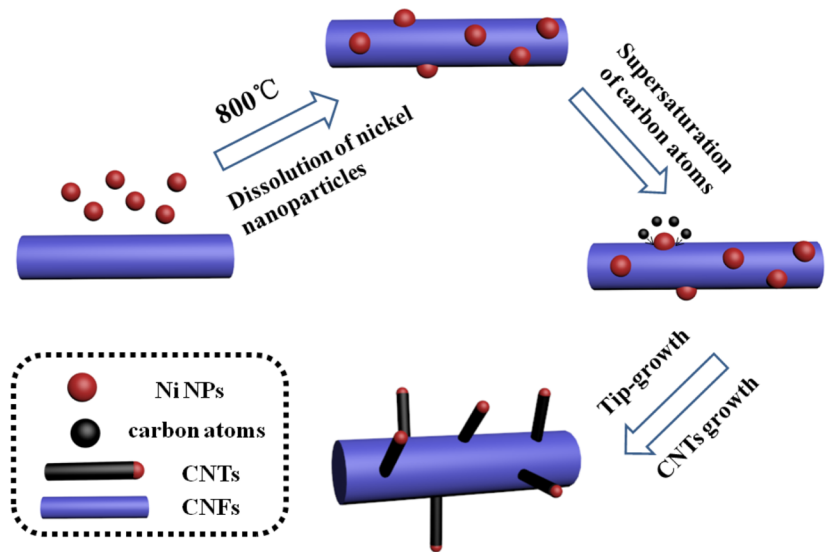
Growth of N-CNTs/N-CNFs hierarchical composites on nickel foam

Nickel foam (NF) was used for this study, which was first cut into pieces of $10 \times 15 \text{ mm}^2$. To eliminate metallic oxides and impurities on the surface of NF, NF was successively dispersed in acetic acid and ethanol solution by ultrasound for 20 min and blown dry with nitrogen (purity, 99.99%). After the pretreatment, the NF was mixed with imidazole according to the mass ratio (1:5) and the above sample was then introduced at the center of the horizontal quartz tube with an outer diameter of 30 mm and an inner diameter of 22 mm. Especially, the inside walls of a horizontal quartz tube were cleaned by using deionized water and ethanol. Before reaching to the reaction temperature of 800 °C, the temperature of the CVD furnace was raised at a ramp rate of 30 °C/min (below 600 °C) and 20 °C/min (between 600 and 800 °C) under a flow rate of 50–150 standard cubic centimeters per minute (sccm). After annealing for 30 min at the reaction temperature, the furnace was cooled to room temperature in the Ar atmosphere at a flow rate of 30 sccm and the black products were taken out of the quartz tube. Finally, the obtained sample was washed in HCl (3 mol/L) solution

Fig. 1 **a** Schematic diagram of the synthesis of N-CNTs/N-CNFs by one-step CVD technique, **b** schematic diagram of the possible tip grow mechanism of CNTs in the hybrid



(a)



(b)

at 80 °C for 2 days to fully remove the nickel substrate yielding the desired N-CNTs/N-CNFs hierarchical composites. Here, we mainly focus on a systematic investigation of the effect of the carrier gas flow rate on the morphology of the sample.

Material characterizations

X-ray diffraction (XRD, Bruker D8 Advance, Billerica, MA, USA) was employed to identify the crystallographic information of the prepared sample. The

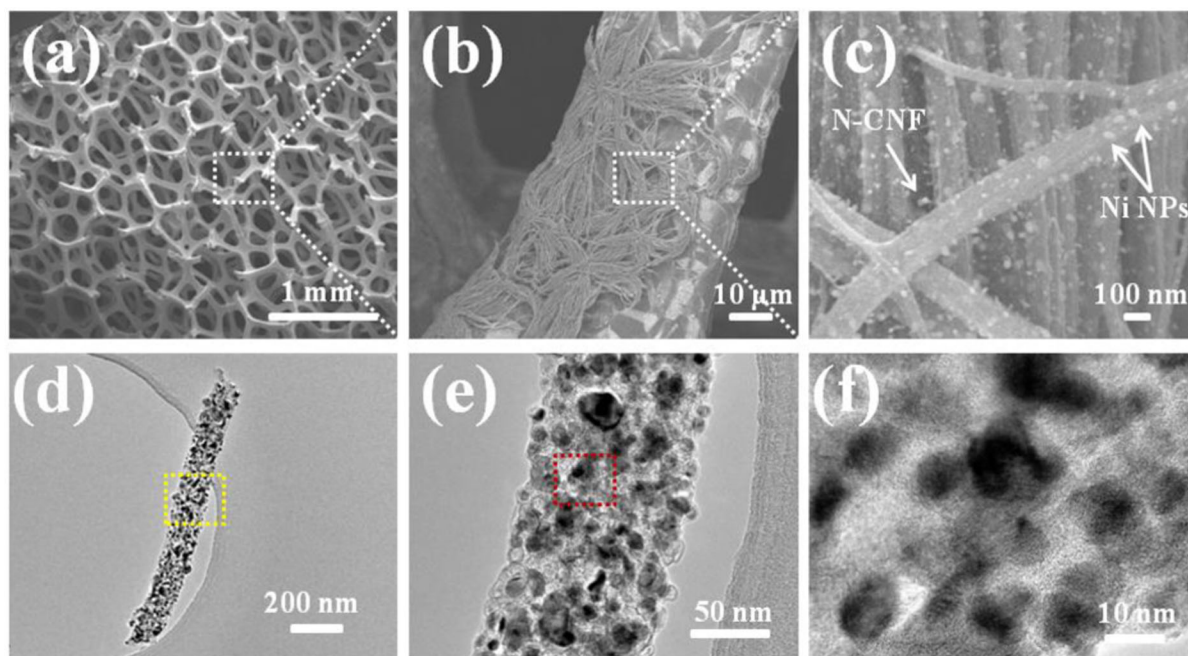


Fig. 2 **a–c** Low- and high-magnification SEM images of the Ni NPs-loaded N-CNFs grown on the surface of nickel foam at the carrier gas flow rate of 50 sccm, **d–f** low- and high-magnification TEM images of the Ni NPs-loaded N-CNFs at the carrier gas flow rate of 50 sccm

morphologies and microstructures were recorded by using field emission scanning electron microscopy (SEM, FEI QUANTA 200F, Hitachi, Tokyo, Japan) and transmission electron microscopy (TEM, JEOL 2010F, Peabody, MA, USA). X-ray photoelectron spectroscopy analyses (XPS, PHI-5700, Ulvac-Phi, Chigasaki, Japan) and Raman spectroscopy (Raman, Horiba Evolution, Tokyo, Japan) were used to analyze the nitrogen doping degree of the sample.

Results and discussion

As shown in Fig. 1a, initially, the imidazole mixed with NF gradually decompose and release many corrosive gases (Ghosh et al. 2010; Minier et al. 1995) such as (H_2 , NH_3) which continually etch the Ni template for producing Ni NPs with the increasing of temperature in the CVD furnace (Ding et al. 2016; Li et al. 2018). As the complete pyrolysis of imidazole, the generated carbon atoms first disperse on the surface of NF, and subsequently dissolve when the temperature approaches 800 °C. Once the reaction temperature begins to decline, a multitude of carbon atoms continuously precipitate on the surface of NF and combine with nitrogen atoms, eventually facilitating the growth of N-CNFs under the

catalytic effect of Ni template. Furthermore, the excessive Ni NPs produced by NF etching result from imidazole pyrolysis adhere to the surface of N-CNFs due to the dissolution of carbon atoms (Ding et al. 2016). Interestingly, N-CNTs simultaneously grow on the already grown N-CNFs by varying the flow rate of carrier gas during the whole synthesis process. As the Ar flow rates increasing, corrosive gases are probably carried out to the CVD furnace, resulting in a decreased concentration of gas etchant. Minjae et al. discovered that a higher concentration of gas (such as H_2) would suppress the decomposition of hydrocarbon precursor, which prevents the supply of carbon source for the growth of CNTs (Jung et al. 2011). Furthermore, the probable “tip-growth” mechanism of N-CNT on the N-CNF surfaces is shown in Fig. 1b. First, the Ni NPs deposit and embed on the surface of N-CNFs due to the great dissolution of carbon atoms, leading to the formation of nucleation sites and CNTs initiate growth at these nucleation sites. As the carbon atoms continue to diffuse to the surface of Ni NPs, subsequently, the carbon atoms rapidly become supersaturated and ultimately, they precipitate from the bottom of the Ni NPs with the structure of CNTs. It is consistent with the previous reports that the CNTs grew on the carbon nanomaterials by the annealing process in the CVD furnace (Guo et al.

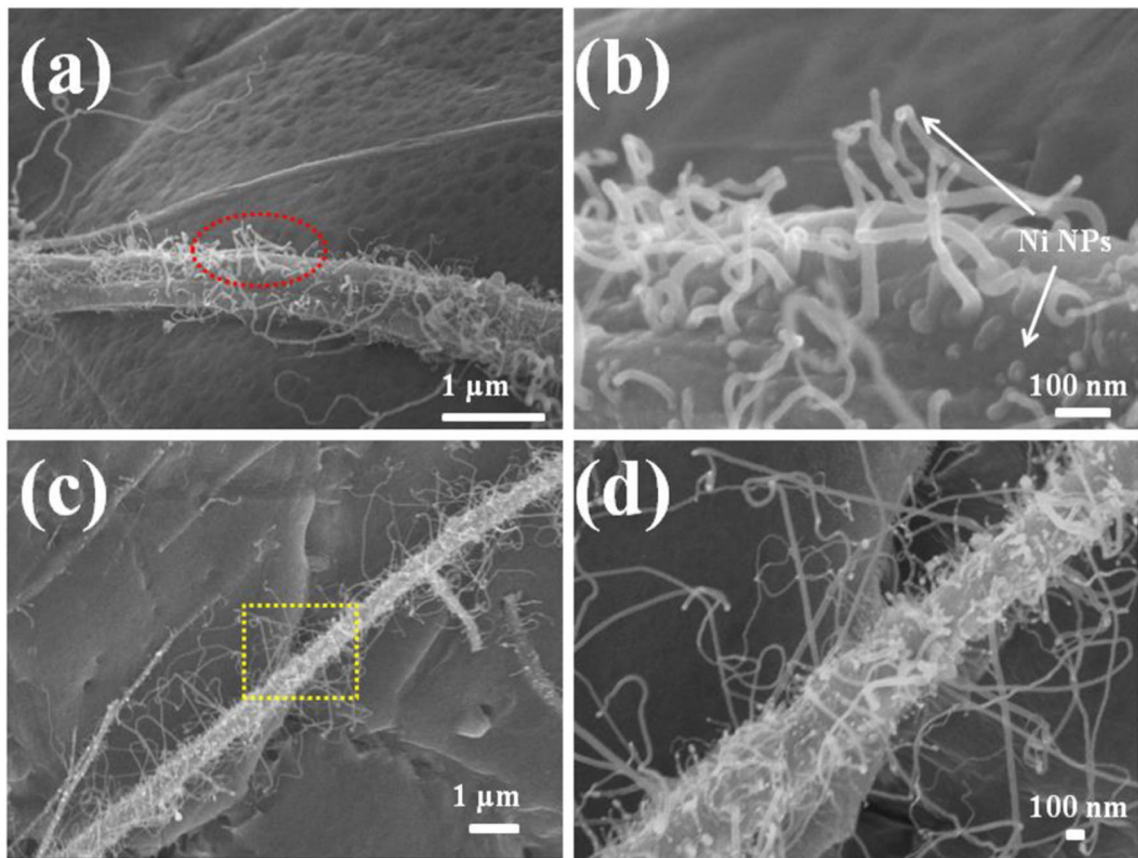


Fig. 3 **a, b** Low- and high-magnification SEM images of the N-CNTs/N-CNFs at the carrier gas flow rate of 100 sccm, **c, d** low- and high-magnification SEM images of the N-CNTs/N-CNFs at the carrier gas flow rate of 150 sccm

2009; Yan et al. 2018). To further investigate the effect of carrier gas flow rate for the 3D hierarchical composites, we carried out controlled experiments by using different carrier gas flow rate (50 sccm, 100 sccm, and 150 sccm) in our case.

SEM analysis

The SEM micrographs of the structures fabricated at a flow rate of 50 sccm are shown in Fig. 2. The 3D interconnected porous structure of NF is displayed in Fig. 2a and we could observe numerous “black wires” on the 3D scaffold, which are N-CNFs (Fig. 2b). As shown in Fig. 2c, N-CNFs with a diameter between 100 and 200 nm are densely grown on the substrate but CNTs are not observed at this flow rate. Furthermore, it is found that large amounts of Ni NPs with a diameter between 10 and 15 nm (Fig. 2f) uniformly dispersed and nearly covered the overall surface of N-CNF (Fig. 2d, e)

result from the violent etching process of carbon precursor gases during the heating stage. And such a strong contact and uniform dispersion of Ni NPs is suitable for the homogeneous growth of N-CNTs. Additionally, the synthesis of Ni NPs-loaded N-CNFs could be fabricated in a one-step CVD technique, which simplifies the procedure compared with the previous similar report (Hou and Reneker 2004).

When the carrier gas flow rate of 100 sccm and a temperature of 800 °C are maintained, SEM analysis in Fig. 3a suggests that curved N-CNTs with a length of about 300 nm could uniformly grow on the surface of N-CNFs film, forming a special 3D carbon structure. This suggests that when the carrier gas flow rate increases from 50 to 100 sccm, more gases etchant (H_2) are carried out to the furnace, increasing precursor decomposition and the subsequent emergence of N-CNTs growth. This extraordinary structure provided additional active sites, beneficial for the application of N-CNTs/N-CNFs hierarchical composites in the electrochemical

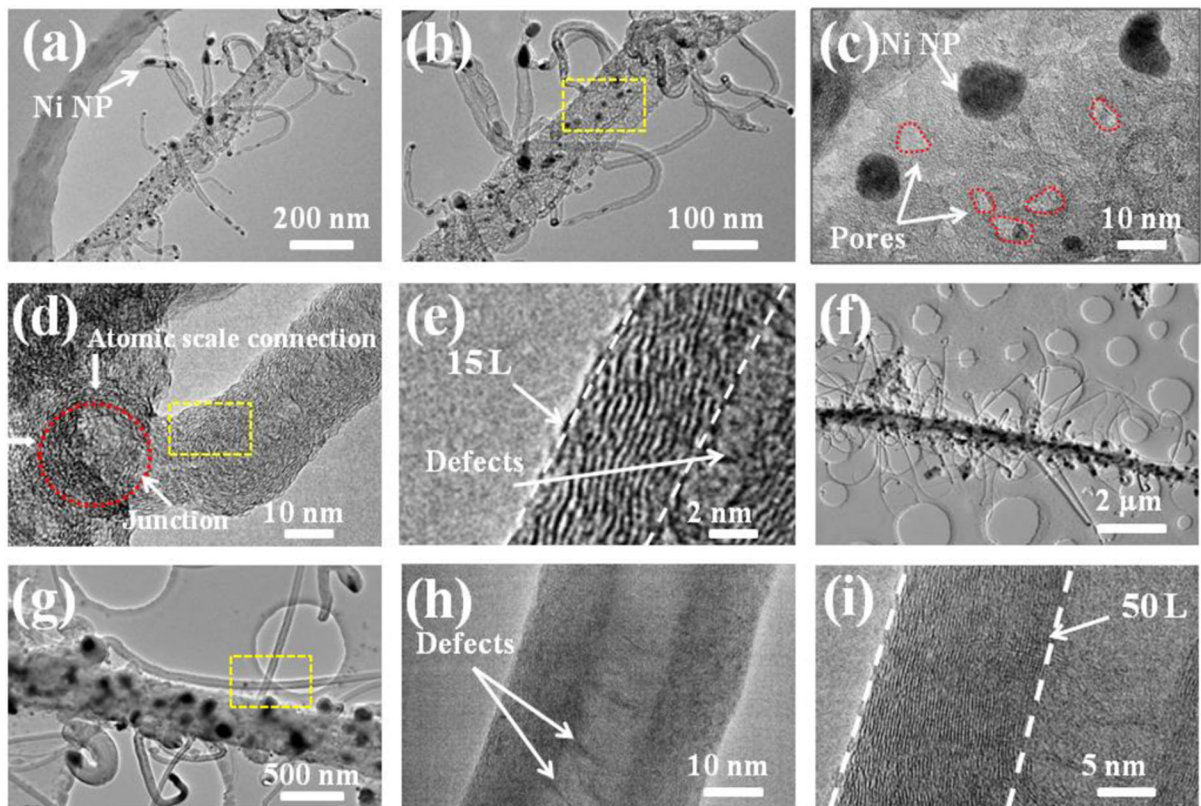


Fig. 4 **a, b** TEM image of N-CNT/N-CNF structure at the carrier gas flow rate of 100 sccm, **c** HRTEM image about Ni NPs taken from the box in **b**, **d** HRTEM image of well-interconnected junction between N-CNT and N-CNF, **e** HRTEM of the defects and the number layers of N-CNT, **f, g** TEM images of N-CNT/N-

CNF structure at the carrier gas flow rate of 150 sccm, **h** HRTEM image about single N-CNT taken from the box in **g**, **i** HRTEM of the defects and the number layers of N-CNT at the carrier gas flow rate of 150 sccm

applications (Zhang et al. 2018). Simultaneously, there are a few dots on the N-CNFs surface and the top of N-CNTs, which are confirmed by TEM to be Ni catalysts (as shown in Fig. 3b). Moreover, at the flow rates of 150 sccm, more carbon atoms from the pyrolysis of feedstock are provided to the supply of CNTs during the synthesis process and consequently, the curled N-CNTs with bigger length (about 2 μm) densely distribute on the surface of N-CNF compared with the flow rate of 100 sccm (Fig. 3c, d). The result demonstrates that the length and density of N-CNTs in N-CNTs/N-CNFs could be controlled by varying or adjusting the carrier gas flow rates in our study.

TEM analysis

At a carrier gas flow rate of 100 sccm, Fig. 4a and b indicate that N-CNT randomly, but tightly, distributed

on the surface of N-CNFs and almost each N-CNT ends with a Ni NP at the tip the nanotubes, revealing the tip-growth model proposed in the Fig. 1b. Notably, the Ni NPs (10–15 nm) embed on the N-CNF surfaces owing to the high solubility of carbon atoms at a high-temperature condition and there are some nanopores (5–10 nm) after removing the Ni NPs (as shown in Fig. 4c). To check the interface structure between the N-CNT and N-CNF, the 3D composite was immersed in an ethanol solution by ultrasound for 30 min before the TEM observations. The result manifests that the N-CNTs are still closely connected with N-CNFs, proving a well-interconnected interaction between the N-CNTs and N-CNFs (as shown in Fig. 4b and f). Furthermore, the HRTEM image (in Fig. 4d) exhibits an atomic resolution junction between the produced N-CNTs and N-CNFs. The root of N-CNTs is well connected with N-CNFs, further confirming the strong interconnection between N-CNTs and N-CNFs. From the high-

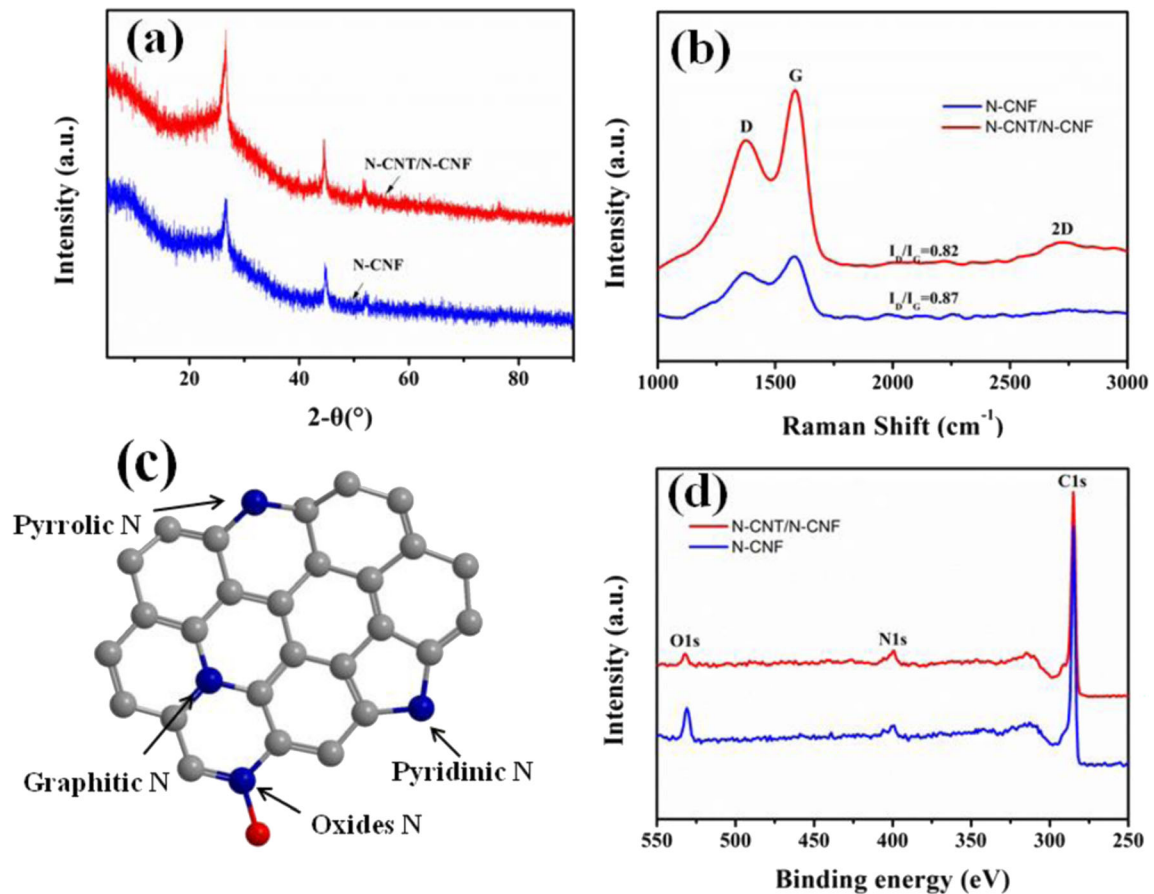


Fig. 5 a, b XRD and Raman spectra images of the N-CNFs and N-CNTs/N-CNFs, c schematic diagram of N-doped carbon matrix with graphitic, pyrrolic, pyridinic, and oxidized N, d XPS spectra of the N-CNFs and N-CNTs/N-CNFs

magnification TEM image (Fig. 4e) of the N-CNT, it exhibits a typical morphology of multiwalled CNT and the diameter of N-CNT and the number of layers is measured to be 15–20 nm and about 15 layers, respectively. Interestingly, many defects are also observed from nanotube, which mainly result from the successful incorporation of nitrogen atoms into CNTs (Sharifi et al. 2012). As the flow rate increases from 100 to 150 sccm, an increased amount of N-CNTs with the bigger length are found attached to the N-CNF surfaces and highly defective sites are also identified in Fig. 4f and h. These

defective sites could effectively improve the electron transport capacity (Yan et al. 2018). However, HRTEM images in Fig. 4h and i illustrate a similar morphology of multiwall CNT with an increased diameter (35–40 nm) and layers (about 50 layers) compared with the low carrier gas flow rate. The comparison suggests that as the flow rate increases, more gas etchant (such as H_2) are carried out to the CVD furnace and do not have abundant gas for the etching process, leading to a decrease in the size of Ni NPs. Huczko (2002) investigated that the diameters and the number of layers in the CNTs were primarily determined by the size of catalysts. Moreover, Aksak and Selamet (2010) further reported that the morphology of carbon nanotube could be tuned by controlling catalyst particle size under different H_2 amounts. Therefore, the higher carrier gas flow rate and the constant reaction temperature (800 °C) could result in the growth of N-CNTs with larger diameters and layers.

Table 1 Atomic composition of N-CNFs and N-CNTs/N-CNTs

Sample	C	N	O
N-CNFs	86.78%	6.44%	6.78%
N-CNTs/N-CNFs	89.52%	7.95%	2.55%

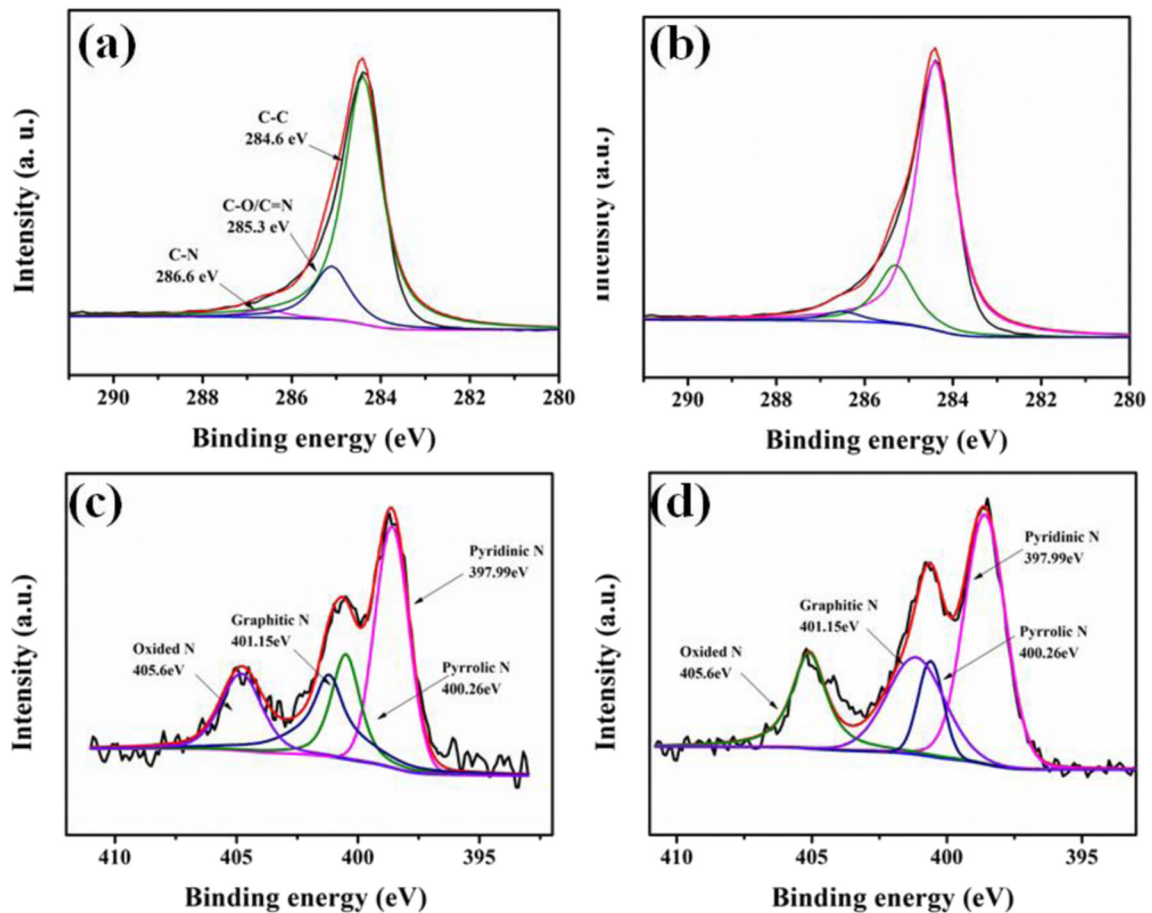


Fig. 6 **a, b** High-resolution C1s XPS spectra of the N-CNFs and N-CNTs/N-CNFs, **c, d** high-resolution N1s XPS spectra of the N-CNFs and N-CNTs/N-CNFs

XRD and Raman analysis

Further characteristics of N-CNTs/N-CNFs composite are conducted by X-ray diffraction (Fig. 5a). The main peaks from both N-CNFs and N-CNTs/N-CNFs locate at approximately 26° , which can be assigned to the (002) crystal plane of graphitic carbon (Fan et al. 2010). Additionally, as shown in the red and blue curve, the other three low characteristic diffraction peaks at 44.5° , 52.5° , and 76° are also visible due to Ni components remaining in the sample after substrate etching (Li et al. 2018). Remarkably, the XRD peak at 26° of N-CNT/N-CNF is sharper than that of N-CNF, indicating the more graphite amount and better crystalline degree after integrating the N-CNT with N-CNF and graphitic crystal structure is restored during the N-doping process (Cai et al. 2017).

Raman spectroscopy is an effective tool to evaluate the crystalline and defects in the sp^2 -hybridized carbon

structure (Fig. 5b). The strong band at about 1580 cm^{-1} , referred to as G band, corresponds to the graphitic E_{2g} modes, which testify the graphitization. The peak at about 1350 cm^{-1} originates from the number of defects in the carbon structure and the intensity ratio of D to G band (I_D/I_G) is associated with the defects in the graphitic carbon. The I_D/I_G ratio (0.82) of N-CNT/N-CNF is lower than the I_D/I_G (0.87) ratio of N-CNF, indicating several defects are reduced during the N-CNT growth. Nevertheless, it can be observed that certain content of defects successful incorporates into the composite in the above TEM results (Fig. 4e, h). This conflict is attributed to the reason that more defects removed from N-CNFs and fewer defects formed in N-CNTs according to the related report (Wang et al. 2015). Moreover, compared with the N-doping materials (I_D/I_G , 0.57–1) using imidazole as carbon and nitrogen source fabricated by Liu et al., our 3D composites include more defects and possess a higher atomic ratio of N (Liu et al. 2011).

XPS analysis

The XPS measurements (Fig. 5d) confirmed that the N-CNTs/N-CNFs are mainly of C, N O. The atomic percentage of N in N-CNTs/N-CNFs (7.95%) is higher than the N-CNFs (6.44%), revealing more nitrogen atoms incorporate into the carbon matrix due to the presence of N-CNTs (Table 1). The atomic percentage of N in N-CNTs/N-CNFs is much higher than that of the previous studies (Guo et al. 2009) (4.8% in nitrogen atomic percentage) about NCNT/CNF by using CVD methods, which is probably attributed to the easier incorporation into carbon matrix of nitrogen from pyrolysis of imidazole. Figure 6a and b display the typical high-resolution XPS spectra of C 1s for N-CNFs and N-CNTs/N-CNFs and they could be deconvoluted into three peaks at 284.6, 285.3, 286.6 eV, which correspond to C–C, C–O/C=N, and C–N, respectively. This result is consistent with the similar N-doped 3D composite reported by Guo et al. (2014). The high-resolution XPS N 1s peak (Fig. 5d) reveals the four types of nitrogen defects, corresponding to pyridinic N (397.99 eV), pyrrolic N (400.26 eV), graphitic N (401.15 eV) and oxidized N (405.6 eV) (Fig. 6c). The high intensity of graphitic N indicates the success of nitrogen doping in the N-CNTs and N-CNFs (Fig. 6d). It is clearly observed that the peak areas of graphitic N in N-CNTs/N-CNFs are significantly higher than those of N-CNFs. This result agrees well with data shown in Fig. 5d. As the predominant bonding configurations of N in N-CNTs/N-CNFs, pyridinic-N leads to more active sites towards ORR, resulting in high electrocatalytic activity from the relevant report (Tian et al. 2014).

Conclusions

In summary, 3D N-CNTs/N-CNFs hierarchical composites have been fabricated by a simple one-step CVD method using imidazole as the carbon and nitrogen source at 800 °C. Interestingly, the N-doped multiwall CNTs are successfully grown on the surface of N-CNFs and the morphology (such as length, diameter, density) of N-CNTs could be controlled by only adjusting the carrier gas flow rates at the constant temperature of 800 °C. The N-CNTs directly grow on the N-CNFs surface, which could not only alleviate the agglomeration and stacking but also serve as the facilitated transport channel for electrolyte ions. Meanwhile, more

defects are observed in the 3D hierarchical composites, which is resulted from the successful incorporation of nitrogen atoms into the carbon matrix. The result indicates that pyridinic-N is the predominant bonding configurations of nitrogen atoms in the N-CNTs/N-CNFs hierarchical composites, resulting in more active sites on the surface of carbon matrix which is beneficial to improve the electrochemical properties and chemical adsorption. As a result, such 3D hierarchical composites probably act as promising materials in energy storage and energy conversion applications, such as fuel cells, batteries, and supercapacitors.

Acknowledgments The assistance of Dr. Zhi-Qun Tian (HRTEM measurements) at Guangxi University is greatly appreciated.

Funding information The National Natural Science Foundation of China (Grants 51762032 and 51462022) and the Natural Science Foundation Major Project of Jiangxi Province of China (Grant 20152ACB20012) provided financial support for this research.

Compliance with ethical standards

Conflict of interest The authors declare that they have no conflicts of interest.

References

- Aksak M, Selamet Y (2010) Carbon nanotube diameter tuning using hydrogen amount and temperature on SiO₂/Si substrates. *Appl Phys A Mater Sci Process* 100:213–222
- Cai J, Wu C, Yang SR, Zhu Y, Shen PK, Zhang K (2017) Templated and catalytic fabrication of N-doped hierarchical porous carbon–carbon nanotube hybrids as host for lithium–sulfur batteries. *ACS Appl Mater Interfaces* 9:33876–33886
- Ding YL, Kopold P, Hahn K, van Aken PA, Maier J, Yu Y (2016) Facile solid-state growth of 3D well-interconnected nitrogen-rich carbon nanotube-graphene hybrid architectures for lithium–sulfur batteries. *Adv Funct Mater* 26:1112–1119
- Dong Q, Wang G, Hu H, Yang G, Qing BQ, Ling Z, Qiu JS (2013) Ultrasound-assisted preparation of electrospun carbon nanofiber/graphene composite electrode for supercapacitors. *J Power Sources* 243:350–353
- Fan ZJ, Yan J, Zhi LJ, Zhang Q, Wei T, Feng J, Zhang ML, Qian WZ, Wei F (2010) A three-dimensional carbon nanotube/graphene sandwich and its application as electrode in supercapacitors. *Adv Mater* 22:3723–3728
- Ghosh K, Kumar M, Maruyama T, Ando Y (2010) Controllable growth of highly N-doped carbon nanotubes from imidazole:

- a structural, spectroscopic and field emission study. *J Mater Chem* 20:4128
- Guo QH, Zhou XP, Li XY, Chen SL, Seema A, Greiner A, Hou HQ (2009) Supercapacitors based on hybrid carbon nanofibers containing multiwalled carbon nanotubes. *J Mater Chem* 19:2810–2816
- Guo QH, Zhao D, Liu SW, Chen SL, Hanif M, Hou HQ (2014) Free-standing nitrogen-doped carbon nanotubes at electrospun carbon nanofibers composite as an efficient electrocatalyst for oxygen reduction. *Electrochim Acta* 138: 318–324
- Hou HQ, Reneker DH (2004) Carbon nanotubes on carbon nanofibers: a novel structure based on electrospun polymer nanofibers. *Adv Mater* 16:69–73
- Huczko A (2002) Synthesis of aligned carbon nanotubes. *Appl Phys A Mater Sci Process* 74:617–638
- Jung M, Yong Eun K, Lee JK, Baik YJ, Lee KR, Wan Park J (2011) Growth of carbon nanotubes by chemical vapor deposition. *Diam Relat Mater* 10:1235–1240
- Kim YS, Kumar K, Fisher FT, Yang EH (2012) Out-of-plane growth of CNTs on graphene for supercapacitor applications. *Nanotechnology* 23:15301–15307
- Kim H, Huang XK, Guo X, Wen ZH, Cui SM, Chen JH (2014) Novel hybrid carbon nanofiber/highly branched graphene nanosheet for anode materials in lithium-ion batteries. *ACS Appl Mater Interfaces* 6:18590–18596
- Landi BJ, Ganter MJ, Cress CD, Dileo RA, Raffaele RP (2009) Carbon nanotubes for lithium ion batteries. *Energy Environ Sci* 2:638–654
- Li HF, Wu F, Wang C, Zhang PX, Hu HY, Xie N, Pan M, Zeng ZL, Deng SG, Wu KV, Dai GP (2018) One-step chemical vapor deposition synthesis of 3D N-doped carbon nanotube/N-doped graphene hybrid material on nickel foam. *Nanomaterials* 8:700
- Liu J, Zhang Y, Ionescu MI, Li R, Sun X (2011) Nitrogen-doped carbon nanotubes with tunable structure and high yield produced by ultrasonic spray pyrolysis. *Appl Surf Sci* 257: 7837–7844
- Liu D, Zhang XP, Sun ZC, You TY (2013) Free-standing nitrogen-doped carbon nanofiber films as highly efficient electrocatalysts for oxygen reduction. *Nanoscale* 5:9528
- Minier, Behrens, JR RB, Bulusu A (1995) Solid-phase thermal decomposition of 2,4-dinitroimidazole (2,4-DIN). *Mrs Proceedings* 418:111–117
- Paraknowitsch JP, Thomas A (2013) Doping carbons beyond nitrogen: an overview of advanced heteroatom doped carbons with boron, sulphur and phosphorus for energy applications. *Energy Environ Sci* 6:2839
- Park M, Jung Y, Kim J, Lee HI, Cho J (2013) Synergistic effect of carbon nanofiber/nanotube composite catalyst on carbon felt electrode for high-performance all-vanadium redox flow battery. *Nano Lett* 13:4833–4839
- Peter KT, Vargo JD, Rupasinghe TP, Jesus DA, Tivanski AV, Sander EA, Myung NV, Cwiertny DM (2016) Synthesis, optimization, and performance demonstration of electrospun carbon nanofiber–carbon nanotube composite sorbents for point-of-use water treatment. *ACS Appl Mater Interfaces* 8: 11431–11440
- Sharifi T, Nitzte F, Barzegar HR, Tai CW, Mazurkiewicz M, Malolepszy A, Stobinski L, Wågberg T (2012) Nitrogen doped multi walled carbon nanotubes produced by CVD-correlating XPS and Raman spectroscopy for the study of nitrogen inclusion. *Carbon* 50:3535–3541
- Sheng ZH, Shao L, Chen JJ, Bao WJ, Wang FB, Xia XH (2011) Catalyst-free synthesis of nitrogen-doped graphene via thermal annealing graphite oxide with melamine and its excellent electrocatalysis. *ACS Nano* 6:4350–4358
- Song JX, Yu ZX, Gordin ML, Wang DH (2016) Advanced sulfur cathode enabled by highly crumpled nitrogen-doped graphene sheets for high-energy-density lithium–sulfur batteries. *Nano Lett* 16:864–870
- Su DW, Cortie M, Wang GX (2017) Fabrication of N-doped graphene-carbon nanotube hybrids from prussian blue for lithium-sulfur batteries. *Adv Energy Mater* 7:1602014
- Tian GL, Zhao MQ, Yu D, Kong XY, Huang JQ, Zhang Q, Wei F (2014) Nitrogen-doped graphene/carbon nanotube hybrids: in-situ formation on bifunctional catalysts and their superior electrocatalytic activity for oxygen evolution/reduction reaction. *Small* 11:2251–2259
- Wang T, Song DF, Zhao H, Chen JY, Zhao CH, Chen LL, Chen WJ, Zhou JY, Xie E (2015) Facilitated transport channels in carbon nanotube/carbon nanofiber hierarchical composites decorated with manganese dioxide for flexible supercapacitors. *J Power Sources* 274:709–717
- Yan Z, Ma LL, Zhu Y, Lahiri I, Hahm MG, Liu Z, Yang SB, Xiang CS, Lu W, Peng Z, Sun ZZ, Kittrell C, Lou J, Choi WB, Ajayan PM, Tour JM (2013) Three-dimensional metal-graphene-nanotube multifunctional hybrid materials. *ACS Nano* 7:58–64
- Yan XL, Li HF, Wang C, Jing BB, Hu HY, Xie N, Wu MH, Vinodgopal K, Dai GP (2018) Melamine as a single source for fabrication of mesoscopic 3D composites of N-doped carbon nanotubes on graphene. *RSC Adv* 8:12157–12164
- Yang J, Wang SY, Ma ZP, Du ZL, Li CY, Song JJ, Wang GL, Shao GJ (2015) Novel nitrogen-doped hierarchically porous coral-oid carbon materials as host matrixes for lithium–sulfur batteries. *Electrochim Acta* 159:8–15
- Zeng LC, Zeng WC, Jiang Y, Wei X, Li WH, Yang CG, Yu YA (2014) Flexible porous carbon nanofibers-selenium cathode with superior electrochemical performance for both Li-se and Na-se batteries. *Adv Energy Mater* 5:1401377
- Zhang SM, Zhang HY, Liu Q, Chen S (2013) Fe-N doped carbon nanotube/graphene composite: facile synthesis and superior electrocatalytic activity. *J Mater Chem A* 1:3302
- Zhang LJ, Jiang YZ, Wang LW, Zhang C, Liu SX (2016) Hierarchical porous carbon nanofibers as binder-free electrode for high-performance supercapacitor. *Electrochim Acta* 196:189–196
- Zhang YZ, Zhang Z, Liu S, Li GR, Gao XP (2018) Free-standing porous carbon nanofiber/carbon nanotube film as sulfur immobilizer with high areal capacity for lithium–sulfur battery. *ACS Appl Mater Interfaces* 10:8749–8757
- Zhao L, Qiu YJ, Yu J, Deng XY, Dai CL, Bai XD (2013) Carbon nanofibers with radially grown graphene sheets derived from electrospinning for aqueous supercapacitors with high working voltage and energy density. *Nanoscale* 5:4902

Publisher's note Springer Nature remains neutral with regard to jurisdictional claims in published maps and institutional affiliations.